2015

Quantification of Ultraprecision Surface Morphology using an Algebraic Graph Theoretic Approach

Prahalad Rao

Satish T. S. Bukkapatnam

Zhenyu (James) Kong

Omer F. Beyca

Kenneth Case

See next page for additional authors

Authors

Prahalad Rao, Satish T. S. Bukkapatnam, Zhenyu (James) Kong, Omer F. Beyca, Kenneth Case, and Ranga Komanduri

Procedia Manufacturing

Volume 1, 2015, Pages 12–26

43rd Proceedings of the North American Manufacturing Research Institution of SME http://www.sme.org/namrc

Quantification of Ultraprecision Surface Morphology using an Algebraic Graph Theoretic Approach

Prahalad Rao[1], Satish Bukkapatnam[2], Zhenyu Kong[3*], Omer Beyca[4], Kenneth Case[5], and Ranga Komanduri[5]

[1]*State University of New York (Binghamton), Binghamton, New York, United States.*
[2]*Texas A&M University, College Station, Texas, United States.*
[3]*Virginia Polytechnic Institute and State University, Blacksburg, Virginia, United States.*
[4]*Fatih University, Istanbul, Turkey*
[5]*Oklahoma State University, Stillwater, Oklahoma, Unites States.*

prao@binghamton.edu, satish@tamu.edu, zkong@vt.edu, ken.case@okstate.edu

Abstract

Assessment of progressive, nano-scale variation of surface morphology during ultraprecision manufacturing processes, such as fine-abrasive polishing of semiconductor wafers, is a challenging proposition owing to limitations with traditional surface quantifiers. We present an algebraic graph theoretic approach that uses graph topological invariants for quantification of ultraprecision surface morphology. The graph theoretic approach captures heterogeneous multi-scaled aspects of surface morphology from optical micrographs, and is therefore valuable for *in situ* real-time assessment of surface quality. Extensive experimental investigations with specular finished (Sa ~ 5 nm) blanket copper wafers from a chemical mechanical planarization (CMP) process suggest that the proposed method was able to quantify and track variations in surface morphology more effectively than statistical quantifiers reported in literature.

Key Words: Surface morphology quantification, semiconductor wafer metrology, chemical mechanical polishing (CMP), copper CMP, graph theory, Fiedler number.

1 Introduction

Surface morphology is a critical determinant of functional integrity in ultraprecision components, such as X-ray mirrors, MEMS devices, semiconductor microchips, etc. (De Chiffre et al., 2003, De Chiffre et al., 2000, Peters et al., 2001, Jiang, 2012). Therefore, quantification of surfaces is essential to effectively track and control morphological modifications to surfaces in ultraprecision manufacturing processes (Jiang et al., 2007, Jiang, 2012). Traditional statistical parameters, such as arithmetic average roughness (Ra, Sa), root mean square roughness (Rq, Sq), and higher statistical

Peer-review under responsibility of the NAMRI Scientific Committee
doi:10.1016/j.promfg.2015.09.025

moments, e.g., skewness (Psk, Ssk) and kurtosis (Pku, Sku) are often incongruous for quantifying ultraprecision surfaces, which typically depict heterogeneous and interdependent morphological features (see Figure 1) each possessing an unique spatial distribution and scaling characteristic (Thomas, 1998). Evident in Figure 1(a) are morphological features, such as scratches, ridges, and pits present on a copper wafer. These features hinder the functional performance of a semiconductor device. The chemical mechanical planarization (CMP) process is used in the semiconductor industry to gradually eliminate these undesirable morphological features (see Figure 1(b)) and yields near-specular surface finish on copper wafers within 9 minutes of processing (Sa ~ 5 nm, Figure 1(c)). However, the measured conventional statistics, such as Sa, Sq, Sz (maximum height), as seen from Figure 1(d) do not track changes to surface morphology. Prior efforts have focused on using a multitude of statistical quantifiers to track surface variations, leading to the so called *parameter rash* (Whitehouse, 1982). For example, a parameter, e.g., Sa, essentially captures the aggregate intensity of the surface topography, while autocorrelation length (Sal) captures their distribution (Jiang, 2012). Parsimonious quantification of ultraprecision surface morphology is therefore a compelling challenge.

Although ultraprecision surfaces may be quantified statistically, salient characteristics of the underlying topography, for instance, the connections between ridges and pits seen in Figure 1(b), termed as *connectedness* by Thomas (Thomas, 1998), are not forthcoming using traditional parameters. While fractal mapping and wavelet decomposition of surfaces have been proposed to quantify multi-scale aspects of surface morphology, these methods often entail estimation of statistics over several length scales, and are therefore computationally intensive and time-consuming (Jiang et al., 2007, Jiang et al., 2008). We show that these limitations can be overcome using an algebraic graph theoretic approach for quantifying ultraprecision surface morphology. The graph theoretic approach by representing the underlying topological relationships is capable of incorporating the effect of diverse morphological features without the need to sift through length scales (Chung, 1997, Fiedler, 1973).

The main contribution of this work is in the graph theoretic representation of ultraprecision surfaces, which allows topological invariants, such as Fiedler number to effectively quantify and track variations in surface morphology. Moreover, it is noted that characterization approaches used for ultraprecision metrology, e.g., laser interferometry (as in Figure 1(a)), scanning electron microscopy (SEM), atomic force microscopy (AFM), etc., can be slow, restricted to assessment of small local areas, cumbersome to implement for large parts, and oftentimes destructive; thus limiting their applicability for real-time *in situ* monitoring scenarios (Jiang, 2012). Existing studies of surface roughness measurement note the benefits of optical methods versus common stylus-based measurement (Sherrington and Smith, 1988b, Sherrington and Smith, 1988a, Shiraishi, 1989, Vorburger and Teague, 1981, Shiraishi, 1981). The most notable of which is the non-contact nature of optical measurement, as well as less measurement variation, due to the evaluation of an area of the surface instead of the line segment obtained by a stylus. Optical and image-based roughness measurement is therefore amenable for on-line monitoring of surface finish. The presented graph theoretic approach, by invoking optical micrographs for quantification of ultraprecision surface morphology, obviates these shortcomings.

The rest of this work is organized as follows: the graph theoretic approach for quantification of ultraprecision surfaces is elucidated in detail in Sec. 2, the approach is validated using numerically generated surfaces, as well as experimentally acquired CMP wafers in Sec. 3 and Sec. 4, respectively, and finally the conclusions are summarized in Sec. 5.

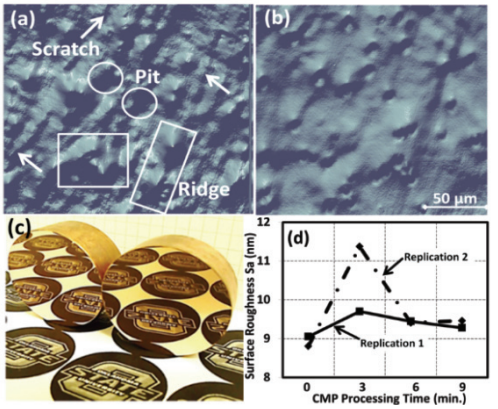

Figure 1: The surface profile of a copper wafer obtained using a laser interferometer (a) before, and (b) after chemical-mechanical planarization (CMP) operations. (a): The surface profile prior to CMP operations shows heterogeneous features, such as scratches, ridges, pits, etc. (b): The surface profile after CMP shows significant improvement in surface morphology within 3 minutes of CMP operations. (c): Specular finish (Sa ~ 5 nm) obtained on CMP processed blanket copper wafers. (d): The mean areal surface roughness (Sa) obtained over 3 minute intervals of CMP for two replications fails to reflect these improvements in surface morphology.

2 Graph-theoretic representation and quantification of surface morphology

Algebraic graph theory approaches have been previously used to describe topological relationships in various physical domains (Shi and Malik, 2000, Von Luxburg, 2007). For example, the Eigen spectra of graphs is used for segmenting (partitioning) an image based on brightness, texture, and color of pixels (Shi and Malik, 2000). However, algebraic graph theoretic image processing techniques are primarily intended towards clustering or segmenting graphs reconstructed from images, which are inhomogeneous in appearance. In comparison, ultraprecision surfaces are typically homogenous, i.e., the various nanoscale morphological features are distributed uniformly over the surface. As we will elucidate herewith, the homogenous morphology of ultraprecision surfaces presents an opportunity for substantial reduction in computational effort.

We now explain the two phased (Figure 2) approach used to realize graph theoretic representation and subsequent quantification of ultraprecision surface morphology from optical micrograph images. Before proceeding, we note that the efficacy of the presented approach is contingent on optical image quality. Therefore, the reliability of results are intrinsically tied to imaging conditions, such as focus, lighting, filtering, environmental aspects, etc. Accordingly, in our experiments, we take care to maintain consistent imaging conditions. Hence, for the CMP process (Sec. 4) we recorded the 3D profiles and optical images of copper wafer surfaces using a laser interferometer operating in the green light region (~ 550 nm wavelength) in order to minimize the effect of variability in lighting conditions.

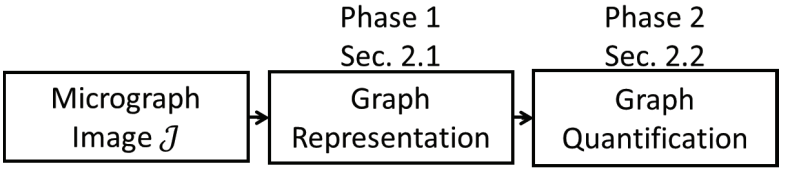

Figure 2: Overview of the methodology for graph theoretic quantification of ultraprecision surfaces.

2.1 Phase 1: Graph representation of optical images scanned using a laser interferometer

Let $\mathcal{I}^{\mathrm{M}\times\mathrm{N}}$ be the matrix representation of a M×N pixels optical micrograph. Due to homogeneity of feature distribution, each row of $\mathcal{I}$ may be treated to be the vertex (or node) of the *undirected* graph $G \equiv (V, E)$ with nodes (vertices) V and edges E (Chung, 1997). For example, in Figure 3 each dot represents a node and each line an edge, with movement possible in either direction along an edge. Such a network graph representation of the surface allows quantification of the *connectivity* aspect among surface features as opposed to merely measuring their statistical characteristics.

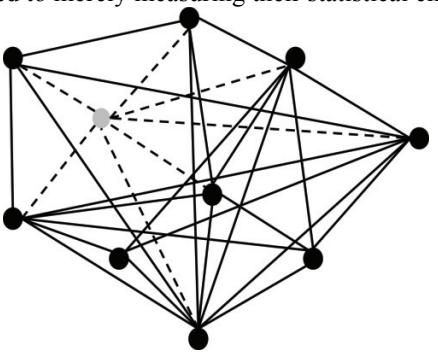

Figure 3: Illustration of an undirected network graph with dots representing nodes (vertices) and lines as edges.

From the M rows (columns could also be used) of $\mathcal{I}$ we construct vectors $F_{(I)}$, $I = \{1,2,\cdots \mathrm{M}\}$, which are row vectors of image pixel values. We compute pairwise comparison metrics $\mathcal{w}_{ij}$ between $F_{(I)}$ using a kernel function Ω (Shi and Malik, 2000).

$$\mathcal{w}_{ij} = \Omega(F_i, F_j) \; \forall \; i, j \in I. \tag{1}$$

We note that these row-wise pixel comparisons are critical for facilitating analysis of homogeneous ultraprecision surfaces as they allow inclusion of features up to a length of N pixels (~ 200 μm in our case) as opposed to only local (< 0.20 μm, ~ 1 pixel) scales; and consequently the computation complexity reduces from a bi-quadratic $\mathcal{O}(\mathrm{M}^2\times\mathrm{N}^2)$ to quadratic $\mathcal{O}(\mathrm{M}^2)$ number. Furthermore, if individual pixel comparisons were to be computed, the resulting graph representation would then be replete with several nodes and edges, and therefore occlude large-scale surface morphology variations. Next, we apply a threshold function Θ which converts $\mathcal{w}_{ij}$ into binary form,

$$\Theta(\mathcal{w}_{ij}) = w_{ij} = \{0,1\} \tag{2}$$

The binary symmetric *similarity matrix* $S = [w_{ij}]$ enshrines the graph G with only those nodes satisfying the threshold condition set in Eqn. (2) being connected, i.e., if an edge exists between any two nodes i and $j \; \forall \; i, j \in I$ then w_{ij} = 1, else w_{ij} = 0. Essentially, G is a convolution of heterogeneous morphological aspects of the surface, such as nano-scratches, pits, and ridges. Therefore, the topology of G inculcates the effect of multi-scale features *simultaneously* without the need to sift through different length scales as typically required in wavelet decomposition and fractal mapping. The topology of the graph G is dependent on the nature of the kernel (Ω) and threshold (Θ) functions. In this work we use the following two kernel and threshold function pairs.

Euclidean Kernel

$$\begin{aligned} \mathcal{w}_{ij} &= \Omega(F_i, F_j) = \left\|F_i - F_j\right\|^2 \forall \; i, j \in I \\ \Theta(\mathcal{w}_{ij}) = w_{ij} &= \begin{cases} 1, & \mathcal{w}_{ij} \geq r \\ 0. & \mathcal{w}_{ij} < r \end{cases} \end{aligned} \tag{3}$$

where, $r = \frac{\sum_{i=1}^{\mathrm{M}} \sum_{j=1}^{\mathrm{M}} \mathcal{w}_{ij}}{\mathrm{M}^2}$

Radial Basis Kernel

$$\begin{aligned} \mathcal{w}_{ij} &= \Omega\left(F_i, F_j\right) = e^{-\left(\frac{\left\|F_i - F_j\right\|}{\sigma_{\mathcal{J}}}\right)^2} \; \forall \; i,j \in I. \\ \mathcal{k}\left(F_i, F_j\right) &= \left\|F_i - F_j\right\|^2; \mathcal{E} = \left[\mathcal{k}\left(F_i, F_j\right)\right] \end{aligned} \tag{4}$$

$$\Theta\left(\mathcal{w}_{ij}\right) = w_{ij} = \begin{cases} 1, & \mathcal{w}_{ij} \leq r \\ 0. & \mathcal{w}_{ij} > r \end{cases}$$

where, $r = \frac{\sum_{i=1}^{\mathrm{M}} \sum_{j=1}^{\mathrm{M}} \mathcal{w}_{ij}}{\mathrm{M}^2}$ and where $\sigma_{\mathcal{J}}$ is the standard deviation of the elements $\mathcal{k}\left(F_i, F_j\right)$ in the Euclidean distance matrix $\mathcal{E}$. The threshold function Θ in Eqn. (2) is a heuristic, manually tuned entity. In the graph segmentation literature, researchers customarily select a hard threshold (r) (Nascimento and De Carvalho, 2011, Shi and Malik, 2000, Von Luxburg, 2007, Schaeffer, 2007, Spielman, 2009, Newman, 2000). The threshold (r) is used to make the similarity matrix *S* sparse and binary. This significantly reduces the computational complexity, particularly the eigen decompositions; to the best of our knowledge, there is no closed form solution that optimizes for r.

Furthermore, Θ is a Heaviside step function for which the threshold (r) is set equal to the average of $\mathcal{w}_{ij}$, i.e., $r = \frac{\sum_{i=1}^{\mathrm{M}} \sum_{j=1}^{\mathrm{M}} \mathcal{w}_{ij}}{\mathrm{M}^2}$, which relaxes the selection of the threshold, because, the threshold can be adaptively estimated contingent on the input image, as opposed to selecting a heuristically determined number. From a signal processing perspective, this relaxation of r is similar in spirit to the universal wavelet threshold proposed by Johnstone and Silverman (Johnstone and Silverman, 1997).

We use this approach for setting the threshold r based on observations from extensive computer simulations (Rao, 2013, Rao et al., 2015 (To Appear)). We found that, if the threshold r was set such that it veered more than ~ 0.1 standard deviations from the mean of $\mathcal{w}_{ij}$, the similarity matrix *S* often became defective (one or more rows in *S* become zero, i.e., signifying an isolated node(s)) or too dense (many edge connections). When the similarity matrix *S* becomes defective, the eigen decompositions required for this work (Eqns. (5) - (9)) cannot be computed. In the scenario where there are dense edge connections, the graph theoretic invariants failed to capture surface morphology variations. Hence, from our empirical knowledge, we selected the threshold r as the average of $\mathcal{w}_{ij}$. This approach for determining r was borne in the light of multiple numerical and experimental studies, e.g., Sec. 3 and Sec.4, where we will show that subtle morphological variations can be captured based on this threshold (Rao, 2013).

Our studies with different types of surfaces revealed that the Euclidean kernel is more suitable for binary (black and white) images, whereas the radial basis kernel is appropriate for gray scale images (Rao, 2013). This is because, the radial basis kernel is essentially a Gaussian filter which normalizes the gray scale texture of the micrograph, therefore $\mathcal{w}_{ij}$ is bounded between (0,1]. In contrast, for the Euclidean kernel function, $\mathcal{w}_{ij}$ is bounded between [0,∞). Consequently, the radial basis kernel is robust to outliers. The emphasis of the subsequent section is to identify a parameter for quantifying the topology of the graph G. Such quantifiers of network topology can be obtained from the *Laplacian Eigen Spectrum* of the graph G in the following manner (Chung, 1997, Fiedler, 1973, Mohar, 1991, Von Luxburg, 2007).

2.2 Phase 2: Quantification of surface morphology using graph theoretic topological invariants

We first compute the *degree* d_i of a node i, which is a count of the number of edges that are incident upon the node, and obtain the diagonal *degree matrix* $\mathcal{D}$ structured from d_i,

$$d_i = \sum_{j=1}^{j=\mathrm{M}} w_{ij} \;\forall\, i,j \in I, \tag{5}$$

$$\mathcal{D} \overset{\text{def}}{\equiv} \mathrm{diag}(d_1, \cdots, d_{\mathrm{M}}). \tag{6}$$

Next, we define the *volume* $\mathcal{V}$ and the *normalized Laplacian* $\mathcal{L}$ of the graph G,

$$\mathcal{V}(G) \overset{\text{def}}{\equiv} \mathrm{tr}(D), \tag{7}$$

$$\mathcal{L} \overset{\text{def}}{\equiv} \mathcal{D}^{-\frac{1}{2}} \times (\mathcal{D} - S) \times \mathcal{D}^{-\frac{1}{2}}. \tag{8}$$

$\mathcal{L}$ is analogous to Kirchhoff matrix encountered in electrical networks (Mohar, 1991). Thereafter, the eigen spectrum of $\mathcal{L}$ is computed as,

$$\mathcal{L}v = \lambda^* v. \tag{9}$$

We note, $\mathcal{L}$ is symmetric positive semi-definite, i.e., $\mathcal{L} \geq 0$, its eigenvalues (λ^*) are non-negative, and bounded between 0 and 2, i.e., $0 \leq \lambda_{\mathrm{i}} \leq 2$. The smallest non-zero eigenvalue (λ_2) is termed the *Fiedler number* and the corresponding eigenvector (v_2) as the *Fiedler vector* (Chung, 1997, Fiedler, 1973). The Fiedler number is related to *Cheeger's constant* $\mathrm{h}(G)$ (also called isoperimetric number), which is a measure of *edge connectivity* of the network G, by the following inequality (Chung, 1997, Fiedler, 1973).

$$\frac{\left(\mathrm{h}(G)\right)^2}{2} \leq \lambda_2 \leq 2\mathrm{h}(G). \tag{10}$$

The graph theoretic *topological invariants*, Fiedler number (λ_2) and Cheeger's constant ($\mathrm{h}(G)$) are often used to quantify the resilience of the graph network to failures (Chung, 1997). Graphs with dense edge connections are typically robust to edge failures, i.e., many edges may have to be removed in order to isolate a node, and characteristically depict larger $\mathrm{h}(G)$ and λ_2 values. In contrast, sparsely connected graphs are relatively easier to disrupt and have lower λ_2 and $\mathrm{h}(G)$ values. This property is evident from the definition of $\mathrm{h}(G)$ (see Ref. (Chung, 1997)). Consider a subset of nodes $A \subset V(G)$ of the graph $G \equiv (V, E)$; if $V(G) - A = \bar{A}$ is the set of all nodes other than A in G and E (G) represents the set of all edges in the graph G then,

$$\mathrm{h}(G) \overset{\text{def}}{\equiv} \min\left\{\frac{|\partial(A)|}{\min\{\mathcal{V}(A), \mathcal{V}(\bar{A})\}}\right\}, \tag{11}$$

$$\partial(A) \equiv \{(x,y) \forall x, y \in E(G) | x \in A,\; y \in \bar{A}\}. \tag{12}$$

Where $\partial(A)$ denotes all edges connecting A with $\bar{A}$. For example, $|\partial(A)| = 7$ for the dashed edges in Figure 3 when the light colored node is the only node in A. In essence, $\mathrm{h}(G)$ accounts for the most sparsely connected node, the severing of whose connections will break the graph in two. From this definition it follows: when the density of edge connections is high, $\mathrm{h}(G)$ and λ_2 will be larger (Fiedler, 1973). From Eqn. (10) – (12), we note that the Fiedler number (λ_2) is not an ordinary statistical parameter, but is indeed physically related to the morphology of a surface. Thus, we have achieved a mapping, $\mathcal{I} \mapsto G$ whose properties are characterized using the Fielder number (λ_2).

In the forthcoming sections, we will validate using numerically generated, as well as experimentally acquired CMP finished surfaces that the graph theoretic topological invariant Fiedler number (λ_2) can track surface morphology variations, which are not captured using traditional statistics-based parameters.

3 Studies with simulated surface topographies

We now demonstrate the graph theoretic approach using two case studies invoking artificially generated surfaces.

- Case 1 (Sec. 3.1): Examines whether the Fiedler number is capable of detecting changes in surface roughness.
- Case 2 (Sec. 3.2): Investigates whether the Fiedler number can distinguish between different types of morphologies resembling surfaces obtained from polishing/fine abrasive finishing processes like CMP.

3.1 Simulation of 3D Surface Profiles with Varying Surface Roughness

In this study we generated 3D rough surfaces with known root mean square surface roughness (Sq). The surfaces have Gaussian distributed peak heights (Figure 4) and are obtained using an FFT-based approach (Wu, 2000). The Sq is varied from 1 μm to 10 μm in integer steps of 1 μm, to emulate the typical surface roughness range of machining processes, such as turning, milling, shaping, etc. (DeGarmo et al., 2003, Sherrington and Smith, 1986); representative examples are shown in Figure 4. Given the inherent nature of the FFT algorithm used for surface generation (Wu, 2000), we note that average surface roughness (Sa) cannot be tightly controlled, however, the Sa is directly proportion to Sq, as exemplified in Figure 4.

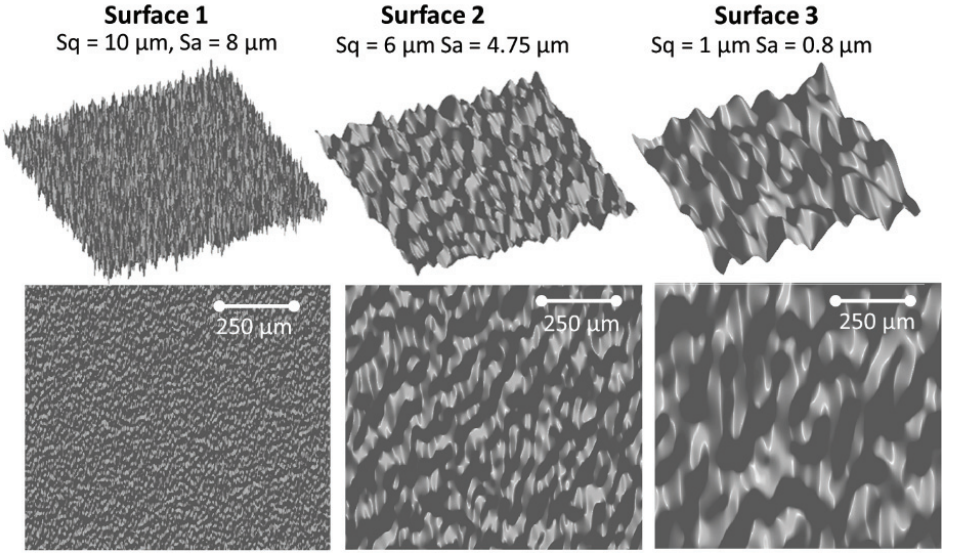

Figure 4: Three representative surfaces with underlying random Gaussian distribution with different surface roughness (Sq and Sa).

In order to estimate the Fiedler number, the top view, akin to an optical image of the generated surfaces (Figure 4, bottom row) is used for analysis; viz., the input image $\mathcal{I}$ in Eqn. (1). For each of the 10 levels of surface roughness, 42 surfaces and accompanying images are obtained, and subsequently analyzed using the Radial Basis Kernel function delineated in delineated in Eqn.(4). The resulting Fiedler number vs. surface roughness (Sq) trend is graphed in Figure 5. The Fiedler number increases with increase in surface roughness, however, the trend is not linear.

Next, we verify whether the difference in (mean) Fiedler number is significant with respect to surface finish. For this purpose we used Tukey's pairwise comparison test, the results from which are visually depicted in Figure 6 (Montgomery, 2008). Based on the Tukey test results, it reasonable to

conclude that the Fiedler number can detect changes in surface roughness with a resolution of ± 1 μm (Sq), however, the sensitivity of the approach is limited for finer surface finish ranges (1 μm – 4 μm, Sq), where the resolution is of the order of ± 2 μm.

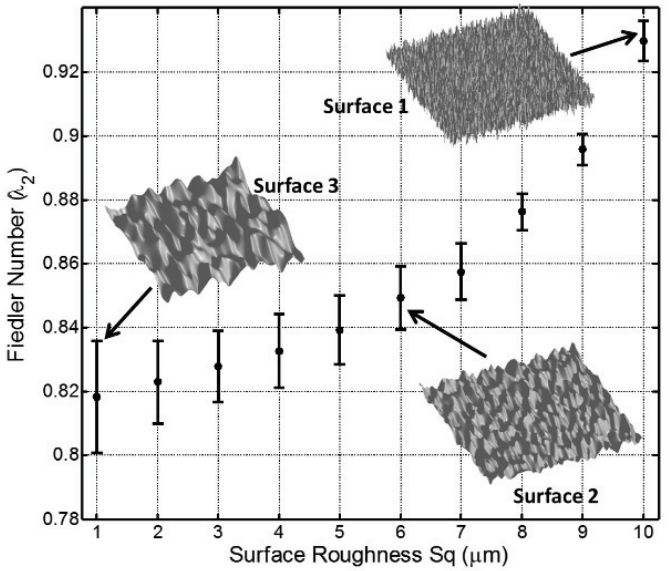

Figure 5: Fiedler number vs. surface roughness (Sq) of artificially generated 3D surfaces. The error bars are ± 1 σ in length.

	Sa	0.80	1.59	2.40	3.20	3.99	4.77	5.59	6.37	7.19	7.97
Sa	Sq	1.00	2.00	3.00	4.00	5.00	6.00	7.00	8.00	9.00	10.00
0.80	1.00	X									
1.59	2.00	0	X								
2.40	3.00	1	0	X							
3.20	4.00	1	1	0	X						
3.99	5.00	1	1	1	0	X					
4.77	6.00	1	1	1	1	1	X				
5.59	7.00	1	1	1	1	1	1	X			
6.37	8.00	1	1	1	1	1	1	1	X		
7.19	9.00	1	1	1	1	1	1	1	1	X	
7.97	10.00	1	1	1	1	1	1	1	1	1	X

Figure 6: The pair-wise differences using Tukey's method with α = 1% level of significance. 1 indicates there is a statistically significant difference (p-val. < 0.01) in Fiedler number between two comparisons (different levels of ρ), 0 indicates that the Fiedler number was not statistically different.

3.2 Simulation of Polished Surface Facets

The aim of this numerical study is to show that the graph theoretic approach can distinguish different types of surface morphologies typically observed in a fine abrasive polishing process, such as CMP. To illustrate the viability of graph-based surface morphology quantification, we patterned the three distinct surface morphologies exemplified in Figure 7(a)-(c). Each of these morphologies has a distinctive type of feature (marked in white) whose density is uniformly set at 3% of total area. These

morphologies mimic some typical semiconductor wafer defects, namely, pitting (Type 1, Figure 7(a)), nanoscale scratch (Type 2, Figure 7(b)), and particle residue/corrosion (Type 3, Figure 7(c)). Fifty-two different instances were simulated for each of these defect types. In this case study, due to the binary nature of simulated surfaces we defined the edge weights using the Euclidean Kernel function (Eqn. (3)).

Plots of the first two eigenvectors, $\mathscr{v}_2$ and $\mathscr{v}_3$ of $\mathcal{L}$ (corresponding to the non-zero eigenvalues λ_2 and λ_3, respectively) for these synthetic surfaces are shown in Figure 7 (d)-(f) where we notice a significant difference in the eigenvector trajectories. The corresponding network graph (only 40 nodes are shown) and Fiedler statistics are plotted in Figure 7(g)-(i). Although the feature density was identical (3%) in all the three cases, the Fiedler numbers (λ_2, Figure 7(j)) are statistically (5% significance level) significantly different. Descriptive statistics concerning the Fiedler number (λ_2) for the three morphology types are shown in Table 1.

Morphology type	Mean Fiedler Number	Std. dev. Fiedler Number	Range Fiedler Number	IQR Fiedler Number
Type 1	0.8172	0.0061	0.0248	0.0084
Type 2	0.7019	0.0461	0.1743	0.0715
Type 3	0.6641	0.0237	0.1052	0.029
Number of data points		52 (for each defect type), 156 total		
Pooled standard deviation		0.0301		
Standard error		0.0042		

Table 1: Descriptive statistics of the Fiedler number measured for different surface morphologies

They were clustered around 0.82 for Type 1 and 0.65 for Type 3, with a statistically significant (p-val. < 0.01) difference in mean Fiedler number for the three cases illustrated. In Type 1 (Figure 7(a)), the pairwise distances $\mathscr{w}_{ij}$ are largely dissimilar (pixel rows look different from each other). Hence, for Type 1 surfaces, $w_{ij} = 1$ (i.e., connected based on our definition) for a large number of nodes. Consequently, the similarity matrix S, as well as the degree matrix $\mathcal{D}$ (Eqn. (5)) is not sparse for this case. This manifests in the rich interconnectivity between nodes seen in Figure 7(g). In contrast, for Type 3, and to a lesser degree for Type 2 surfaces (Figure 7(h) and (i), respectively), the network is well pruned, i.e., $w_{ij} = 0$ for many nodes. As a result, we recognize from Figure 7(h) and (i) that the nodes of the graph for Type 2, and particularly Type 3 surfaces, are not as well connected compared to Type 1. Hence, it is relatively easy to isolate a node for Type 2 and Type 3 surfaces in comparison to Type 1 surfaces. Therefore, from the definition of $\mathrm{h}(G)$ in Eqn. (11), one expects the Fiedler number to be higher for Type 1 relative to Types 2 and 3. This case study illustrates that the Fiedler number is sensitive to variations in surface morphology, which are not captured using statistical parameters such as defect density. Nonetheless, the converse is not presumed, i.e., the simulated surface morphologies may have the same Fiedler number if the defect densities were allowed to vary. We now apply the graph theoretic approach for characterizing CMP processed blanket copper (Cu) wafers.

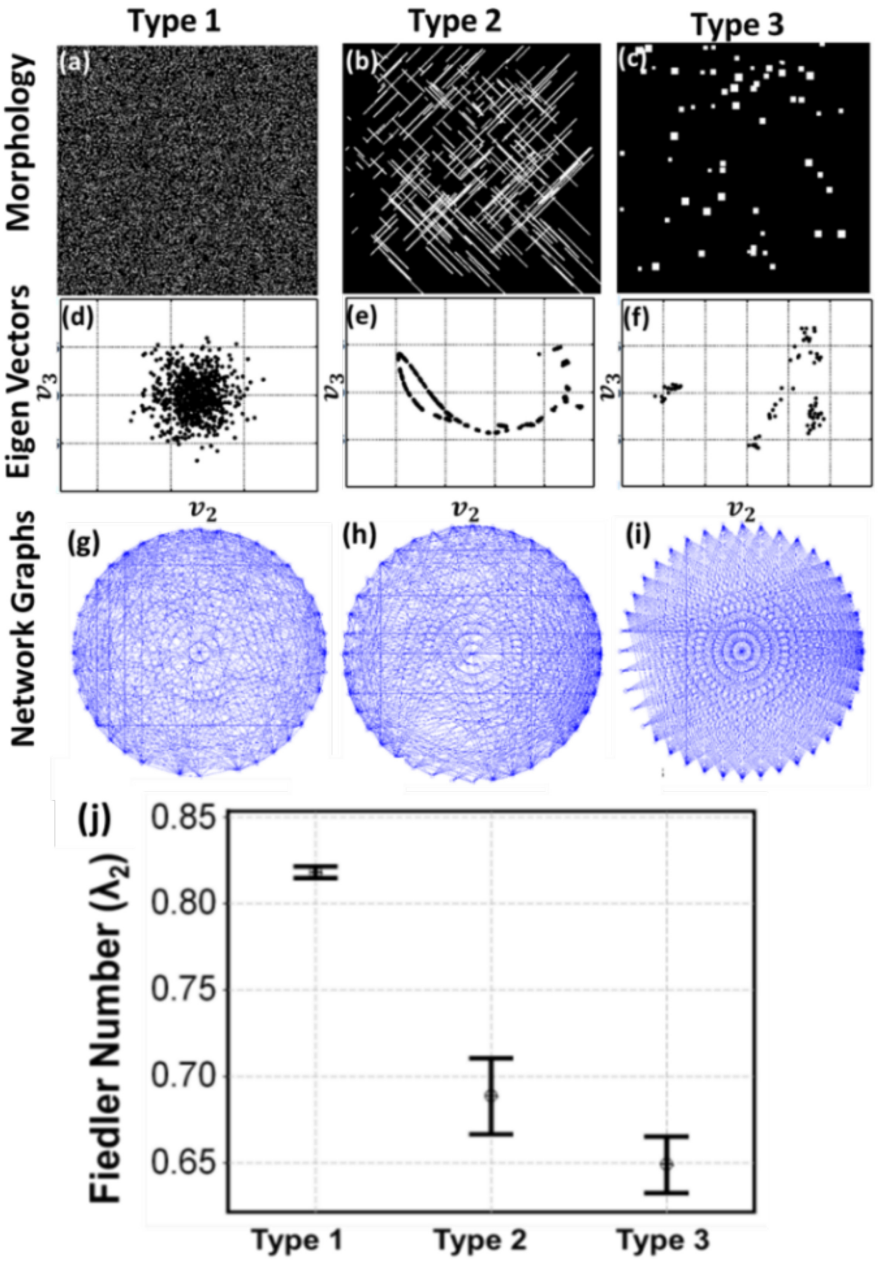

Figure 7: (a) – (c): Studies with three types of simulated surface morphologies features with the density of features maintained at 3%. (d) – (f): The eigenvectors map corresponding to morphologies represented in (a) – (c), respectively. (g) – (i): corresponding network graphs (40 nodes only show). (j): Fiedler statistics estimated for the three types of simulated morphologies.

4 Application to CMP processed blanket copper wafers and validation using conventional surface roughness measurements

Blanket copper wafers (dia. 40.625 mm) are CMP processed in three intervals, each lasting 3 minutes, for realizing specular surface characteristics with Ra in the range of 5 – 10 nm (e.g., Figure 8) (Rao et al., 2014). We recorded the surface profile (e.g., Figure 1(a) and (b)) and corresponding optical images at six randomly selected positions on the wafer after every 3 minutes of polishing.

Figure 8: Blanket copper wafers with specular finish obtained after 9 minutes of CMP using 70 nm colloidal silica slurry.

Surfaces shown in Figure 9(a1) and (b1), are representative optical images for a 3 minute and 9 minute CMP processed wafer, respectively. The corresponding network graph obtained using the Euclidean kernel function (after conversion to black and white using a Canny filter (Canny, 1986)) from these optical images are shown in Figure 9(a2) and (a3), respectively. Similarly, Figure 9 (b2) and (b3) show the network graphs obtained using the radial basis kernel. The mean Fiedler number (λ_2) estimated from optical micrographs of Cu wafer surfaces across different polishing intervals using both Euclidean and radial basis kernels are shown in Figure 9 (c1) and (c2)) and also tabulated in Table 2. The mean Fiedler number is observed to reduce with progressive CMP stages. The difference in mean Fiedler number across CMP intervals was statistically significant at the 5% confidence level; except between 3 minutes and 6 minutes intervals for the radial basis function kernel. This is visually depicted in terms of the network graphs in Figure 9 (a2, b2) and (a3, b3), where there is a marked sparseness in edges going from 3 minute to 9 minute CMP stages, implying that some nodes can be easily isolated, and hence the Fiedler number is smaller for the 9 minute CMP stage.

Furthermore, we compared these results with locally measured conventional statistics, such as Sa, Sq, Sz, feature density (obtained using a heuristically determined Canny filter (Canny, 1986)), and power spectral density (PSD) of the surface profile. After a CMP interval, conventional statistical parameters were estimated from a set of approximately 200 random sampled wafer locations at different areal scales. Some of these locally estimated statistics are shown in Figure 10(a)-(d) for samples measuring 25 µm × 25 µm. Estimation of local statistics in this manner requires sifting through several scale levels and is therefore computationally demanding. Estimation of local statistics in this manner necessitates sifting through several scale levels; it is computationally demanding and requires involved analysis, and hence it is not practically viable in a production scenario.

The correlation ρ between the Fiedler number and local estimates of conventional areal parameters (Table 3) was assessed to be the range of ~ 80% to 98%. This implies that the Fiedler number is sensitive to changes in surface morphology and depicts the same trend as locally estimated statistical parameters without requiring expensive computations stemming from sifting through length scales. For instance, estimating the local parameters shown in Figure 10 for a surface profile measurement (e.g., Figure 9(a)) required repeated computations over 20 areal scales starting from 100 µm × 100 µm and going to 5 µm × 5 µm. This expended approximately 20 minutes of computation for each CMP wafer. In contrast, the illustrated graph theoretic approach does not need such scale-based estimations;

the computational overhead reduces to less than 5 minutes. For instance, estimating the local parameters shown in Figure 10 for a surface profile measurement (e.g., Figure 9(a)) required repeated computations over 20 areal scales starting from 100 μm × 100 μm and going to 5 μm × 5 μm. This expended approximately 20 minutes of computation for each surface profile – entailing over 2 hr. of analysis for a set of 6 profiles obtained for a CMP stage. In contrast, the illustrated graph theoretic approach does not need such scale-based estimations; affords global quantification (250 μm × 250 μm) wafer surface morphology; and the computational overhead reduces to less than 5 minutes. More pertinently, the estimation of statistical parameters was done from 3D profiles obtained using a laser interferometer, which is a time consuming process. Instead the Fiedler number (λ_2) is calculated directly from optical images, which are tractable, non-contact, and quicker to obtain in production scenarios.

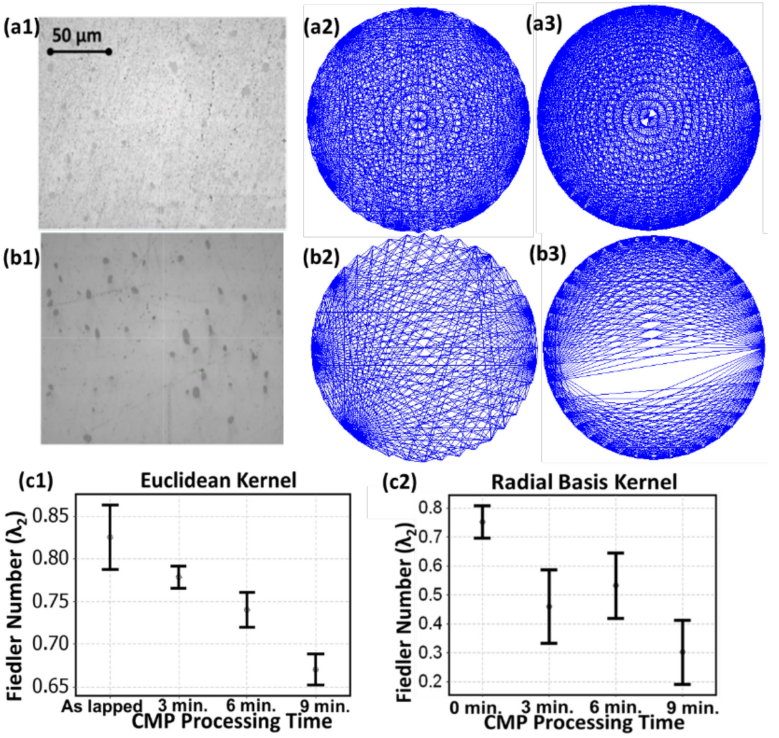

Figure 9: Results from graph representation of CMP processed surfaces. Optical micrographs of copper wafer surfaces (a1) before CMP operations, and (b1) after 9 minutes of CMP operations; corresponding network graphs using Euclidean kernel are shown in (a2) and (b2), and radial basis kernel in (a3) and (b3), respectively. (c1), and (c2) Fiedler statistics vs. CMP processing time for Euclidean and radial basis kernels, respectively.

Polishing Stage	Euclidean Kernel		Radial Basis Kernel	
	$\bar{\lambda}_2$	σ_{λ_2}	$\bar{\lambda}_2$	σ_{λ_2}
As lapped	0.81	0.036	0.75	0.066
3 minutes	0.76	0.024	0.46	0.152
6 minutes	0.72	0.034	0.49	0.151
9 minutes	0.66	0.017	0.33	0.148

Table 2: Fiedler number estimates across different CMP stages using Euclidean and radial basis kernel functions.

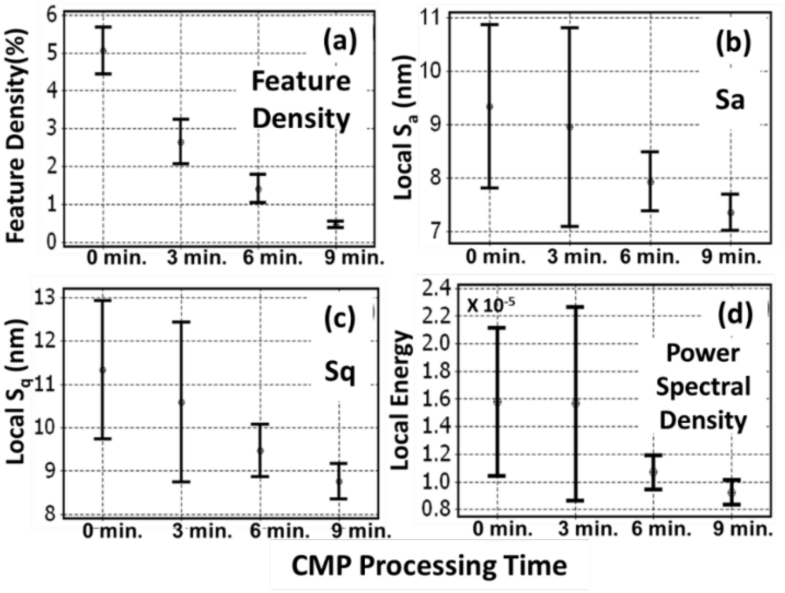

Figure 10: Conventional statistics vs. CMP processing time samples measuring 25 μm × 25 μm; ~ 200 samples were taken at each CMP interval. (a): percentage feature density. (b): arithmetic mean roughness (Sa). (c): root mean squared roughness (Sq). (d): power spectral density (PSD).

Parameter	ρ Euclidean Kernel	P Radial Basis Kernel
Local maximum height of surface texture Sz (nm)	0.92	0.98
Feature density (%)	0.94	0.93
Local root mean square roughness Sq (nm)	0.99	0.87
Local arithmetic mean roughness Sa (nm)	0.99	0.81
Local PSD energy content from 2D fast Fourier transform	0.94	0.77

Table 3: Correlation coefficient (ρ) for various locally estimated (25 μm × 25 μm area) conventional parameters when compared with mean Fiedler number obtained across CMP stages.

5 Conclusions

In closure, we have presented an algebraic graph theoretic approach for quantifying ultraprecision surface morphology, which overcomes some of the lacunae associated with conventional statistics-based surface metrology quantifiers. We have demonstrated that, on invoking the algebraic graph theoretic topological invariant Fiedler number of the graph reconstructed from the images, surface morphology of ultraprecision components, such as semiconductor wafers, can be assessed from optical micrographs; and consequentially enabling timely, non-contact, and *in situ* metrology of such surfaces. Being able to elucidate these topological relationships may usher a more perspective exposition of surfaces whose morphology is difficult to quantify, such as patterned substrates, soft materials, biological tissues, etc., which can be useful for gaining insights into unresolved problems in tribology and contact mechanics (Thomas, 1998). Specific outcomes from this work are as follows:

1. 3D surface profiles with surface roughness (Sq) in the range of 1 μm to 10 μm were numerically generated (Sec. 3.1). The Fiedler number (λ_2) showed an increasing trend, albeit nonlinear, with increase in surface roughness.

2. The graph theoretic topological invariant, Fiedler number (λ_2) was assessed to be a more effective quantifier of surface morphology in comparison to conventional defect count measurement. Three different defect distributions, with identical defect counts and bearing a close resemblance to actual CMP surfaces, were simulated (Sec. 3.2). The Fiedler numbers estimated for the three cases were significantly different (p-val < 0.01), indicating that the Fiedler number is more responsive to changes in surface morphology.
3. The approach was verified against experimentally acquired CMP wafer surface micrographs and topography scans (obtained using a laser interferometer). We demonstrate that nanoscale aspects of CMP polished wafers, which were not adequately captured using conventional statistical metrology parameters, can be tracked using the graph theoretic invariant Fiedler number (λ_2).
4. We validated the estimated Fiedler number (λ_2) obtained at different CMP stages by comparison with locally sampled conventional surface characterization parameters, such as Sa, Sq, Sz, PSD, and percentage defect count. The correlation coefficient ρ between conventional parameters and Fiedler number was estimated to be in the range of 75 – 98% for all combinations tested.

Acknowledgements

The authors acknowledge the generous support of the NSF via the following grants: CMMI 1266331, 1437139, 1432914, 1401511, IIP 1355765, IOS 1146882. One of the authors (SB) also wishes to acknowledge AT&T Professorship (Oklahoma State University) and Rockwell International professorship (Texas A&M University) for additional support. The authors dedicate this article to the fond memory of Dr. Ranga Komanduri (1942-2011), a scholar and a mentor, whose presence would be deeply missed.

References

Canny, J. 1986. A computational approach to edge detection. *IEEE Transactions on Pattern Analysis and Machine Intelligence***,** 679-698.

Chung, F. R. K. 1997. *Spectral Graph Theory,* Providence, RI, American Mathematical Society.

De Chiffre, L., Kunzmann, H., Peggs, G. & Lucca, D. 2003. Surfaces in precision engineering, microengineering and nanotechnology. *CIRP Annals-Manufacturing Technology,* 52**,** 561-577.

De Chiffre, L., Lonardo, P., Trumpold, H., Lucca, D., Goch, G., Brown, C., Raja, J. & Hansen, H. N. 2000. Quantitative characterisation of surface texture. *CIRP Annals-Manufacturing Technology,* 49**,** 635-652.

Degarmo, E., Black, J. T. & Kosher, R. 2003. *Material and Processing in Manufacturing,* New York, NY, John Wiley and Sons.

Fiedler, M. 1973. Algebraic Connectivity of Graphs. *Czechoslovak Mathematical Journal,* 23**,** 298-305.

Jiang, X. 2012. Precision surface measurement. *Philosophical Transactions of the Royal Society A: Mathematical, Physical and Engineering Sciences,* 370**,** 4089-4114.

Jiang, X., Scott, P. & Whitehouse, D. J. 2008. Wavelets and their applications for surface metrology. *CIRP Annals - Manufacturing Technology,* 57**,** 555-558.

Jiang, X., Scott, P. J., Whitehouse, D. J. & Blunt, L. 2007. Paradigm shifts in surface metrology. Part 2 : The current shift. *Proceedings of the Royal Society A: Mathematical, Physical and Engineering Science,* 463**,** 2071-2099.

Johnstone, I. M. & Silverman, B. W. 1997. Wavelet threshold estimators for data with correlated noise. *Journal of the Royal Statistical Society: Series B (Statistical Methodology),* 59**,** 319-351.

Mohar, B. 1991. The Laplacian spectrum of graphs. *Graph Theory, Combinatorics, and Applications,* 2**,** 871-898.

Montgomery, D. C. 2008. *Introduction to Statistical Quality Control*, John Wiley & Sons.

Nascimento, M. C. & De Carvalho, A. C. 2011. Spectral methods for graph clustering–A survey. *European Journal of Operational Research,* 211**,** 221-231.

Newman, M. W. 2000. *The Laplacian Spectrum of Graphs.* MS Thesis, University of Manitoba.

Peters, J., Bryan, J. B., Estler, W. T., Evans, C., Kunzmann, H., Lucca, D. A., Sartori, S., Sato, H., Thwaite, E. G., Vanherck, P., Hocken, R. J., Peklenik, J., Pfeifer, T., Trumpold, H. & Vorburger, T. V. 2001. Contribution of CIRP to the Development of Metrology and Surface Quality Evaluation during the last fifty years. *CIRP Annals - Manufacturing Technology,* 50**,** 471-488.

Rao, P., Beyca, O., Bukkapatnam, S., Kong, Z. J., Case, K. E. & Komanduri, R. 2015 (To Appear). A Graph Theoretic Approach for Quantification of Surface Morphology and its Application to Chemical Mechanical Planarization (CMP) Process. *IIE Transactions (Accepted, in-press)*.

Rao, P. K. 2013. *Sensor-based monitoring and inspection of surface morphology in ultraprecision manufacturing processes*. PhD Dissertation, Oklahoma State University.

Rao, P. K., Bhushan, M. B., Bukkapatnam, S. T. S., Zhenyu, K., Byalal, S., Beyca, O. F., Fields, A. & Komanduri, R. 2014. Process-Machine Interaction (PMI) Modeling and Monitoring of Chemical Mechanical Planarization (CMP) Process Using Wireless Vibration Sensors. *IEEE Transactions on Semiconductor Manufacturing,* 27**,** 1-15.

Schaeffer, S. E. 2007. Graph clustering. *Computer Science Review,* 1**,** 27-64.

Sherrington, I. & Smith, E. H. 1986. The significance of surface topography in engineering. *Precision Engineering,* 8**,** 79-87.

Sherrington, I. & Smith, E. H. 1988a. Modern measurement techniques in surface metrology: part I; stylus instruments, electron microscopy and non-optical comparators. *Wear,* 125**,** 271-288.

Sherrington, I. & Smith, E. H. 1988b. Modern measurement techniques in surface metrology: part II; optical instruments. *Wear,* 125**,** 289-308.

Shi, J. & Malik, J. 2000. Normalized cuts and image segmentation. *IEEE Transactions on Pattern Analysis and Machine Intelligence,* 22**,** 888-905.

Shiraishi, M. 1981. In-process measurement of surface roughness in turning by laser beams. *Journal of Engineering for industry,* 103**,** 203-209.

Shiraishi, M. 1989. Scope of in-process measurement, monitoring and control techniques in machining processes—Part 2: In-process techniques for workpieces. *Precision Engineering,* 11**,** 27-37.

Spielman, D. A. 2009. Spectral graph theory. *Lecture Notes, Yale University*.

Thomas, T. R. 1998. Trends in surface roughness. *International Journal of Machine Tools and Manufacture,* 38**,** 405-411.

Von Luxburg, U. 2007. A tutorial on spectral clustering. *Statistics and Computing,* 17**,** 395-416.

Vorburger, T. & Teague, E. 1981. Optical techniques for on-line measurement of surface topography. *Precision Engineering,* 3**,** 61-83.

Whitehouse, D. J. 1982. The parameter rash — is there a cure? *Wear,* 83**,** 75-78.

Wu, J.-J. 2000. Simulation of rough surfaces with FFT. *Tribology International,* 33**,** 47-58.